Journal of Materials Chemistry C

ROYAL SOCIETY OF CHEMISTRY

PAPER

View Article Online
View Journal | View Issue

Cite this: J. Mater. Chem. C, 2020, 8, 15393

Towards highly conducting bicarbazole redox polymer films with plateau-like conductivities†

Claudia Malacrida,[a] Yushi Lu,[a] Klaus Dirnberger,[a] Sergio Gámez-Valenzuela,[b] M. Carmen Ruiz Delgado [b] and Sabine Ludwigs *[a]

Chemical doping of redox polymer films based on triphenylamine (PVTPA), phenylcarbazole (PVPhCbz) and carbazole (PVCbz) pendant redox units is performed with different concentrations of $FeCl_3$ solutions. Analogies to *in situ* electrochemical doping show that stable crosslinked dimer containing redox polymer films are created. The conductivity behavior of the doped films is analyzed and the charge carrier species are identified by UV-Vis-NIR spectroscopy. In particular the behavior of PVCbz upon doping is unique: transparent films with conductivities as high as 2×10^{-2} S cm^{-1} are found over a large range of $FeCl_3$ concentrations. Such plateau-like conductivity – also encountered upon electrochemical doping – is a phenomenon, usually only found for conjugated polymers such as poly(3-hexylthiophene). PVTPA and PVPhCbz on the other hand show bell-shape behavior with maximum conductivities reaching 10^{-3} S cm^{-1} for a limited range of dopant concentrations. The stability (induced by crosslinking) and the transparency make the layers applicable as transparent electrodes or hole-transport layers in opto-electronic devices. The observed results are discussed in the context of mixed valence conductivity with high conductivities only accessible when a certain amount of dications coexists with radical cation species. While PVTPA and PVPhCbz follow the classical findings of the model, a favorable π-stacking tendency of bicarbazole dimers seems to strongly improve efficient communication between the redox sites in the three dimensionally connected redox polymer films. Our results indicate that the nature of charge propagation of redox and conjugated polymers is closer than usually discussed in the literature which can be mainly attributed to intermolecular interactions throughout the films. Last but not least we want to highlight the strength of *in situ* electrochemical techniques to identify charged species and potential-dependent conductivity regions which help targeting optimized chemical doping.

Received 30th June 2020,
Accepted 3rd September 2020

DOI: 10.1039/d0tc03090b

rsc.li/materials-c

Introduction

The intrinsic electronic conductivity upon chemical and electrochemical doping combined with their solution processability, lightweight and synthetic versatility has made conducting polymers very appealing candidates in a wide number of applications including thermoelectric devices, transparent electrodes as well as in energy storage applications.[1–5]

Based on the nature of charge propagation conducting polymers can be subdivided into two main groups, namely redox and conjugated polymers.[6] In the case of redox polymers, electronic conductivity is sustained by electron hopping, which is essentially an electron exchange reaction between localized redox active units, whereas for conjugated polymers the motion of delocalized electrons occurs in intra and inter conjugated chains. Mechanisms of conductivity, and in particular, correlations with the redox state of the polymers have been the subject of studies since decades;[7,8] a useful technique for this purpose, with Murray[9,10] and Zotti[11] as pioneers, is *in situ* conductance coupled to cyclic voltammetry. Despite several studies in the literature,[7,8,12] a general mechanism for describing the potential-dependent conductivity behavior of conducting polymers has not yet been found. A mixed-valence conductivity model can be successfully employed for describing the conductivity profile of pure redox systems which is typically characterized by narrow potential regions of conductivity with a characteristic peak or bell-shape.[7,8,10,13,14] Experimentally it remains non-trivial to find the optimum doping level to reach maximum conductivities, furthermore conductivities typically remain rather low.[8]

Conjugated systems such as poly(3-hexylthiophene) and poly(ethylenedioxythiophene) are on the other hand characterized

[a] IPOC-Functional Polymers, Institute of Polymer Chemistry, University of Stuttgart, Pfaffenwaldring 55, 70569 Stuttgart, Germany. E-mail: sabine.ludwigs@ipoc.uni-stuttgart.de
[b] Department of Physical Chemistry, University of Málaga, 29071 Málaga, Spain

† Electronic supplementary information (ESI) available. See DOI: 10.1039/d0tc03090b

by a sigmoidal shape and broad conductivity region when polarons and bipolarons are present.[15–18] This type of behavior was also tried to be rationalized in terms of a mixed valence conductivity model[19,20] in contrast to the bipolaron model.[21] For P3HT we have recently developed an *ex situ* electrochemical doping approach that allows precise tuning of the doping level of films and allows reaching maximum conductivities of 224 S cm^{-1} over broad doping potential ranges.[22] These systems gain from interchain interactions due to the planar backbones of P3HT. One example for a conjugated polymer which behaves rather as a localized redox system is n-type poly{[*N*,*N*′-bis-(2-octyldodecyl)-naphthalene-1,4,5,8-bis(dicarboximide)-2,6-diyl]-*alt*-5,5′-(2,2′-bithiophene)} (PNDI2OD-T_2) which has maximum conductivities in the mixed valence states of the neutral/radical anion and radical anion/dianion respectively.[23,24]

In this work we show that also pure redox polymer systems can give typical characteristics of conjugated polymers, such as plateau-conductivities. For this we present a doping conductivity study on polymers based on triphenylamine, polyvinyltriphenylamine (PVTPA), and carbazole redox active pendants, polyvinylphenylcarbazole (PVPhCbz) and polyvinylcarbazole (PVCbz) (Scheme 1). Following an oxidative dimerization approach of the triarylamine and carbazole redox units[25–29] cross-linked polymer thin films can be generated with dimeric redox-active units *N*,*N*,*N*′,*N*′-tetraphenylbenzidine (TPB), 9,9′-diphenyl-9*H*,9′*H*-3,3′-bicarbazole (BPhCbz) and 9,9′-diethyl-9*H*,9′*H*-3,3′-bicarbazole (BCbz), respectively.

An analysis of the doping behavior of such systems is very important for applications where the system is employed in a doped state, for example during the charging/discharging process in batteries[30] or where the materials are employed in highly doped states *e.g.* in hole-transport layers (HTLs) or transparent electrodes in perovskite solar cells and organic light emitting diodes.[31–33]

The manuscript is structured as follows: In the first part of the manuscript we analyse the chemical doping of PVTPA,

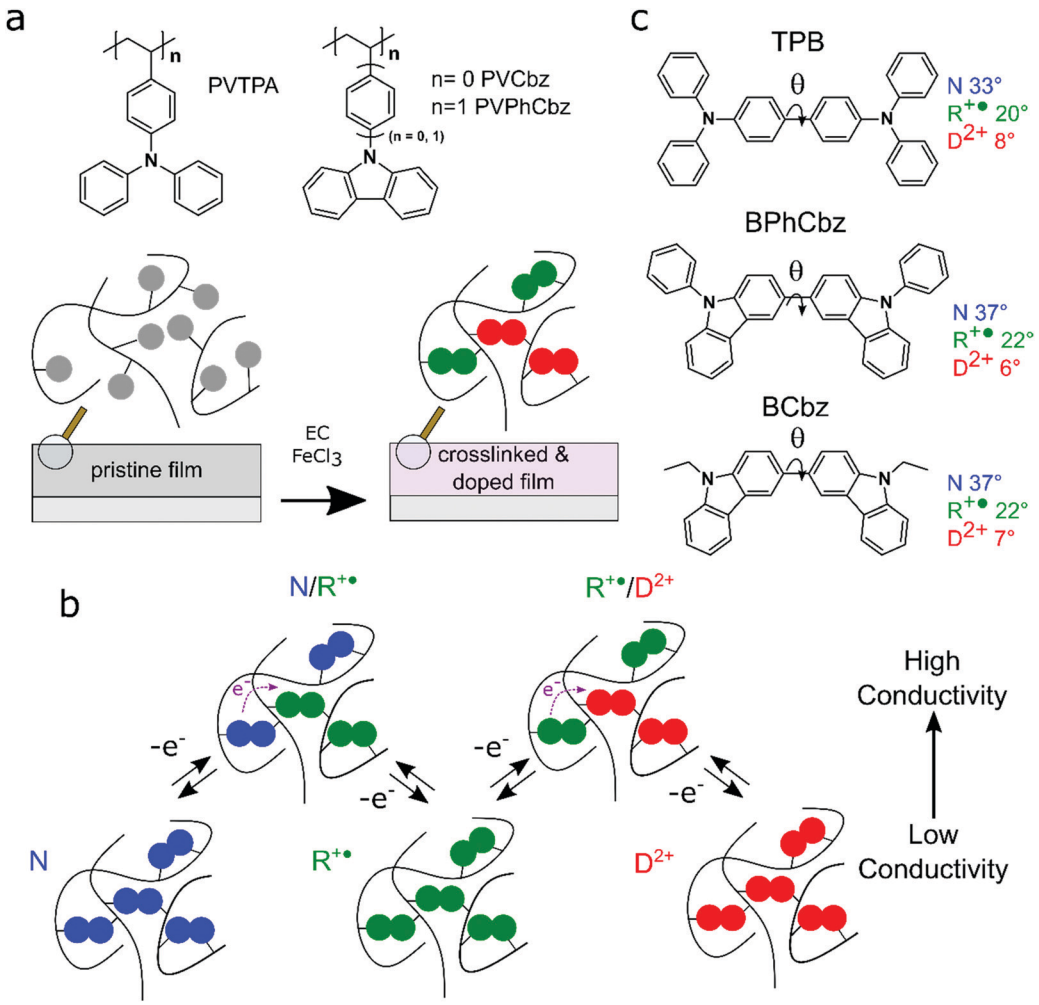

Scheme 1 (a) Representation of the crosslinking process as a result of oxidative coupling by chemical or electrochemical doping of the redox active TPA and Cbz to the respective TPB and BCbz dimer units in films of the three polymers PVTPA, PVPhCbz and PVCbz. (b) Representation of the mixed-valence conductivity mechanism between dimeric species in the neutral (N, blue), radical cation ($R^{+\bullet}$, green) and dication (D^{2+}, red) states with maximum conductivity obtained in mixed valence states N/$R^{+\bullet}$, and $R^{+\bullet}$/D^{2+}. (c) DFT-optimized (B3LYP/6-31G** level in acetonitrile) dihedral angles (θ) of TPB, BPhCbz and BCbz dimers, respectively, in different states of oxidation, color code as in (b).

PVPhCbz and PVCbz redox polymer films upon oxidation with $FeCl_3/CH_3CN$ solutions. The chemical doping of the polymer films, which takes place with concurrent crosslinking of the redox-pendant units in the films, is studied by 4-point probe conductivity experiments and UV-Vis-NIR spectroscopy. In the second part of the manuscript the chemical doping results are compared with *in situ* spectroelectrochemical and *in situ* conductance measurements performed on electrochemically crosslinked and doped polymer films. This set of experiments allows us to follow the trends in conductance as a function of oxidation potential in correlation to the evolution of the neutral, radical cation and dication state, respectively.[7,12,18] Based on previous findings[34] the chemical and electrochemical doping results are interpreted within the mixed valence conductivity model (Scheme 1b) and the differences encountered between the polymers are discussed in terms of intermolecular interactions.

We find that PVCbz (often abbreviated as PVK in the literature) gives conductivities as high as 10^{-2} S cm^{-1} over a large range of doping concentrations and electrochemical potentials. PVTPA and PVPhCbz achieve conductivities of 10^{-3} S cm^{-1} in rather narrow concentration and potential ranges. The increased chemical stability resulting from crosslinking together with the transparency of the resulting doped layers makes them interesting candidates for HTLs and transparent electrodes in optoelectronic applications.

Experimental section

Sample preparation

Sample preparation was performed by spin coating the polymers from chloroform solution (10 mg mL^{-1}) at room temperature (samples for chemical doping: 1000 rpm s^{-1} on float glass substrates (1 cm^2); samples for electrochemical characterization: 2000 rpm). After casting, all polymer films were annealed at 150 °C for 1 h. Atomic Force Microscopy (Dimension Icon, Bruker) and profilometry (Dektak 150, Veeco) were used to measure film thickness. Typical film thicknesses of the chemically doped samples were around 90–100 nm and of the samples employed for electrochemical characterization were around 50 nm.

Chemical doping

Chemical doping and the related characterization (UV-Vis-NIR and conductivity measurements) were performed in a nitrogen filled glovebox to avoid dedoping effects otherwise observed (ESI†). Chemical doping was performed by exposing the substrates to anhydrous iron(III) chloride ($FeCl_3$) in acetonitrile as dopant solutions. The doping process was controlled by varying the concentration of the dopant and its exposure time. The excess of dopant was removed from the sample by spinning at 3000 rpm for 1 min. Immediately after doping, the sheet resistivites of the polymer films were measured using the four-point-probe technique (Signatone SP4 probe head, linear arrangement of tips, spacing = 1 mm, and Keithley 2636B SourceMeter). The samples were also analysed by UV-Vis-NIR spectroscopy.

Electrochemical measurements

Electrochemical measurements were performed with an Autolab PGSTAT204 potentiostat (Metrohm) at room temperature under an Argon atmosphere. A three-electrode glass cell equipped with a Pt plate as a counter electrode (CE) and an AgCl-coated silver wire as a pseudo reference electrode (RE) were employed. As working electrodes (WE) 1 cm × 1.5 cm Au (vacuum deposited on glass slides over 5 nm of adhesion Cr layer; 50 nm Au layer) slides and 5 μm spacing Pt interdigitated electrodes (Dropsens, Metrohm) were used. Prior to usage, the electrodes were cleaned by sonication with water, isopropanol and acetone, 10 min each. For all the electrochemical measurements a 0.1 M CH_3CN solution (Sigma Aldrich) with Bu_4NPF_6 as a supporting electrolyte (Sigma Aldrich) was employed; the electrolyte solution was deaerated through argon bubbling before the measurements. All potentials were referenced to the formal potential of the $Fc|Fc^+$ reference redox couple, measured under the same conditions of the analytes. The redox active polymer films were crosslinked by potentiodynamically cycling at oxidative potentials with a scan-rate of 20 mV s^{-1} recording the voltammetric signal for three subsequent cycles in 0.1 M Bu_4NPF_6/CH_3CN.

In situ spectroelectrochemical experiments

In situ spectroelectrochemical experiments were performed using an Autolab PGSTAT204 potentiostat (Metrohm) and a Zeiss UV-Vis spectrometer coupled with a MCS621 Vis II spectrometer cassette and a CLH600F lamp or a Zeiss UV-Vis-NIR spectrometer coupled with a MCS621 Vis II and a MCS611 NIR 2.2μ spectrometer cassette and a CLH600F lamp. The measurements were conducted in a custom-made three-electrode quartz cell employing a Pt wire as a counter electrode (CE), an AgCl coated Ag wire as a (pseudo)reference electrode (RE) and polymer-coated 5 μm interdigitated (IDE) Pt electrodes (Dropsens) as working electrodes (WE). The measurements were performed under an Ar atmosphere and all the potential values were referenced to the formal potential of the $Fc|Fc^+$ redox couple. *In situ* spectroelectrochemical measurements were conducted with a scan rate of 20 mV s^{-1} and potential steps of 10 mV, with simultaneous recording of electrochemical data points and UV-Vis-NIR spectra every 0.5 s.

In situ conductance experiments

In situ conductance experiments were performed in parallel to the CV measurements. Interdigitated Pt electrodes from DropSens (comb distance = 5 μm) were used as the working electrodes. The CV experiments were performed at room temperature under an argon atmosphere using an Autolab PGSTAT101 potentiostat (Metrohm) (potentiostat 1) with a Pt wire as a CE and an AgCl-coated Ag wire directly immersed into the electrolyte solution as a pseudoreference electrode. Additionally, a constant bias (E_d) of 10 mV was applied between the combs of the interdigitated electrode using a second potentiostat (μStat400, DropSens) measuring the current (I_d) which is flowing between the two combs of the interdigitated electrodes as a function of the potential in the CV measurement.

With the help of two resistors (Heka interface), both current signals are galvanostatically separated in order to allow conducting both the CV measurements and to measure the *in situ* conductance simultaneously. The conductance values G were calculated from the measured current flowing between the combs according to Ohm's law $G = \frac{1}{R} = \frac{I}{V}$. Electrolyte solutions (0.1 M Bu_4NPF_6/CH_3CN) were deaerated by argon bubbling before use. Conductance values are given as conductance change (ΔG) with respect to the conductance of the materials in the neutral state (background current non-negligible in the experimental setup) (Fig. S11, ESI†).

Results and discussion

Conductivity behavior upon chemical doping

The chemical doping of PVTPA, PVPhCbz and PVCBz thin films was conducted by a sequential solution doping method. The low cost oxidizing agent $FeCl_3$ (anhydrous) was used because of a high standard oxidation potential of 1.47 V *vs.* $Fc|Fc^+$ of the Fe(III)/Fe(II) redox couple in acetonitrile.[32–35] $FeCl_3$ has already been used to polymerize and dope triarylamines and carbazoles in the literature.[28,36–39] Furthermore, chemical oxidation with $FeCl_3$ and electrochemical oxidation lead to similar oxidation products which is important for a direct comparison between chemically and electrochemically oxidized samples in this manuscript.[15,37,40]

All chemical oxidation measurements reported in the manuscript were performed in a nitrogen filled glovebox. Thin films of the polymers were covered with 50 μL of the oxidant in acetonitrile, which is an orthogonal solvent for the polymers, and excess of dopant was removed by spincoating. The doping process was controlled by varying the concentration of the dopant [0.1 to 4 mg mL^{-1} in the case of triphenylamine polymer and 1 to 10 mg mL^{-1} for the carbazole polymers] and its exposure time. In order to follow the chemical doping process, and in particular to identify the nature of charge carriers responsible for the measured conductivities of each film, UV-Vis-NIR spectra were recorded.

Conductivity data of PVTPA, PVPhCbz and PVCbz films doped with $FeCl_3$ solutions for 10 s are presented in Fig. 1. Maximum conductivities of $(1.0 \pm 0.1) \times 10^{-3}$ S cm^{-1} and $(6.8 \pm 1.1) \times 10^{-4}$ S cm^{-1} for PVTPA (Fig. 1a) and PVPhCbz (Fig. 1b) are registered upon doping with 2 mg mL^{-1} and 5 mg mL^{-1} solutions, respectively. By analyzing the dependency of the conductivity of PVTPA and PVPhCbz on the $FeCl_3$ concentration, a bell shape trend is observed, with conductivity decreasing after reaching the maximum. PVCbz (Fig. 1c) on the other hand is the polymer presenting the highest conductivities and gives values up to 10^{-2} S cm^{-1} for $FeCl_3$ concentrations in a large concentration range from 3 to 10 mg mL^{-1}. For all three polymers maximum conductivities measured for films after 60 s doping time were similar but were reached already at lower oxidant concentrations. This strongly suggests a diffusion controlled process[41] (ESI,† Fig. S2, S6 and S7). Fig. 1 further shows selected UV-Vis-NIR spectra for the 3 polymers in the neutral non-doped form (black continuous line), in the state of the highest conductivity (purple dashed line) and at the highest doping concentration (black dotted line). For the complete set of measurements we refer to the ESI† (Fig. S3 and S5).

In the case of PVTPA (Fig. 1d) the pristine polymer exhibits a neutral band with a maximum of 322 nm, this fits very well with the absorption wavelength reported for the pure triphenylamine (TPA) compound.[42] At 2 mg mL^{-1} $FeCl_3$ concentration one can distinguish bands with maxima at 479, 707, 804 and >1100 nm. At the highest concentration of 5 mg mL^{-1} a small band at 479 nm and a more distinct band around 804 nm are visible. In all doped samples, a peak maximum at 360 nm is observed which is associated with the absorption of the dopant $FeCl_3$, which overall hampers band assignments to the polymer species in this wavelength range (in particular, neutral dimerized species: TPB, BPhCbz and BCbz (see the discussion below)).[42,43]

PVPhCbz (Fig. 1e) seems to be characterized by a similar absorption behavior as PVTPA in relation to conductivity. The neutral polymer film has an absorption maximum at 328 nm.[44] The highest conductivity was registered for the 5 mg mL^{-1} doped sample where the characteristic film absorption presents maxima at 428 nm, 797 nm and 1024 nm. For the 10 mg mL^{-1} doped film the band at 797 nm is dominant.

In the case of PVCbz doping (Fig. 1f), the absorption of the neutral polymer has a maximum at 332 nm. The conductivity values do not show significant variations above 3 mg mL^{-1} over the whole concentration range explored, also the absorption behavior is quite similar. One can identify a band around 422 nm, as well as a rather broad band above 600 nm with a shoulder around 770 nm in the films doped with 5 and 10 mg mL^{-1}. The spectra show overall less pronounced variations when compared with the ones registered for chemically doped PVTPA and PVPhCbz. It can be noted that the films are overall quite transparent which could be useful for application as a transparent electrode. The charge carrier assignment upon chemical oxidation will be elucidated with the help of electrochemical studies in the following (Fig. 3 and Table 1).

Electrochemical studies of PVTPA, PVPhCbz and PVCbz films

To better understand the different conductivity behavior observed for the three polymers – despite their structural similarities – *in situ* electrochemical studies were conducted for PVTPA, PVPhCbz and PVCbz thin polymer films. The *in situ* combination of cyclic voltammetry with conductance and UV-Vis-NIR spectroscopy allows the assignment of the charge carriers to the associated conductance response of the polymer films when tuning their oxidation/doping level.

Preparation of poly(TPB), poly(BPhCbz) and poly(BCbz)

For all three polymer films, first cyclic voltammetry was performed with a scan-rate of 20 mV s^{-1} in 0.1 M Bu_4NPF_6/CH_3CN electrolyte solutions (Fig. 2a), all given potentials are referenced with respect to the internal standard $Fc|Fc^+$. In the first forward

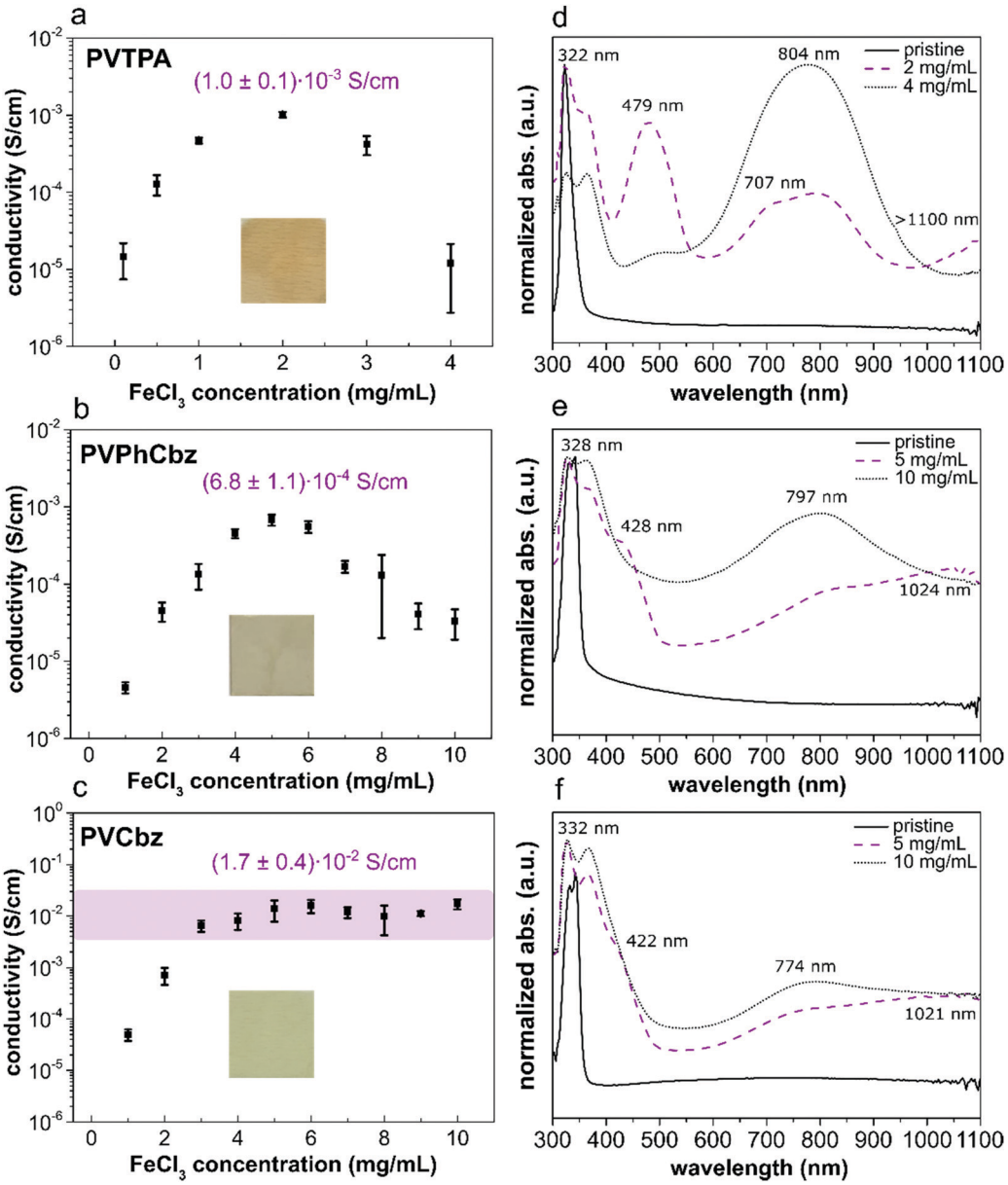

Fig. 1 (a–c) Conductivities for PVTPA (a), PVPhCbz (b) and PVCbz (c) films measured after sequential doping with $FeCl_3/CH_3CN$ doping solutions for 10 s. The photographs in the insets correspond to the films in their highest conducting state (dimensions of ~ 1 cm^2) and indicate transparency. (d–f) UV-Vis-NIR normalized absorption spectra of the polymer films PVTPA (d), PVPhCbz (e), and PVCbz (f) in their neutral state (black continuous line), in the state where the highest conductivity was measured (purple dashed line), and in the state where the highest $FeCl_3$ concentration was applied (black dotted line).

Table 1 Characteristic UV-Vis-NIR absorption maxima upon electrochemical doping of poly(TPB), poly(BPhCbz) and poly(BCbz) and chemical oxidation by $FeCl_3$ of PVTPA, PVPhCbz and PVCbz

	EC doping of poly(TPB), poly(BPhyCbz) & poly(BCbz)			Chemical doping of PVTPA, PVPhCbz & PVCbz		
Species	$\lambda_{max\ N}$ (nm)	$\lambda_{max\ R^{+\bullet}}$ (nm)	$\lambda_{max\ D^{2+}}$ (nm)	$\lambda_{max\ N}$ (nm)	$\lambda_{max\ R^{+\bullet}}$ (nm)	$\lambda_{max\ D^{2+}}$ (nm)
TPA	—	—	—	322	—	—
TPB	352	476 (1083)	741	—	479 (>1100)	804
PhCbz	—	—	—	328		
BPhCbz	342	429 (1004)	751	—	428 (1024)	797
Cbz				332		
BCbz	326	402 (999)	761	–	422 (1021)	777

cycle of the voltammetric experiment all films show an irreversible oxidation peak assigned to the one-electron oxidation of the redox active pendant unit to the radical cation state. The peak potentials for the irreversible oxidation (E_{cl}) are at 0.63 V for PVTPA, 0.84 V for PVPhCbz and 0.79 V for PVCbz, respectively. For a detailed description of the oxidation mechanism of arylamines and carbazoles we refer to the literature[27,45–47] and present a complete reaction mechanism in the ESI† (Fig. S8). The reaction involves the one-electron oxidation of the redox units generating radical cations, which are highly unstable due to the high spin density localized at the phenyl *para* position in triarylamines and the position 3 of the carbazole units. The species undergo an irreversible dimerization generating *N*,*N*,*N*′,*N*′-tetraphenylbenzidine (TPB) in the case of PVTPA and 3-3′-bicarbazole (BCbz) in the case of PVPhCbz and PVCbz, respectively. The as-generated films will accordingly be called poly(TPB), poly(BPhCbz) and poly(BCbz) in the following.

The second voltammetric cycle shows in all cases a decrease of the oxidation onset, as expected by the increased conjugation following the coupling reaction. The CV patterns of the generated poly(TPB) and poly(BPhCbz) show two reversible and partially overlapping oxidation peaks which are assigned to the one electron oxidation to the radical cation at half-wave potentials of $E^{1/2}$ = 0.39 V ($TPB^{+\bullet}$) and 0.65 V ($BPhCbz^{+\bullet}$) and, at higher potentials of oxidation to the subsequent one electron oxidation to the dication state with $E^{1/2}$ = 0.53 V (TPB^{2+}) and 0.89 V ($BPhCbz^{2+}$). In comparison to the other polymers poly(BCbz) does not show clear and separated oxidation waves, but rather a broad reversible oxidation signal up to potentials of 0.9 V, with characteristics more typical of conjugated systems such as P3HT. Differential pulsed voltammetry (DPV) of a poly(BCbz) thin film (Fig. S10, ESI†) also shows a similar behavior. An onset potential of 0.26 V corresponding to a HOMO of −5.36 eV is measured for the poly(BCbz) film.

Based on the literature results[27,36,40] we expect that the oxidation and coupling of the redox pendant groups in acetonitrile stops at the level of dimerization and no superior oligomers are generated. The dimerization of redox-active pendants in the polymer films occurs both in inter- and intra-polymer chains and results in crosslinked networks.[25] The crosslinking reaction leads to an increased stability towards dissolution, in particular for solvents such as acetone and THF for which the pristine films are completely soluble. No significant variations in the CV shape are observed between the second and all following subsequent voltammetric cycles, suggesting that the coupling reaction might be concluded after the first cycle. In fact, a further increase of the conjugation length with the number of cycles (formation of higher oligomers) would result in progressive lowering of the oxidation onset which was not observed here. Electrogenerated poly(TPB), poly(BPhCbz) and poly(BCbz) films were characterized by *in situ* UV-Vis-NIR and conductance for further comparison with the chemical oxidation experiments.

Poly(TPB)

The evolution of the spectra of poly(TPB) during the forward cycle of the CV is presented in Fig. 2b and c (see also Fig. S13, ESI†). The neutral polymer film shows an absorption maximum at 352 nm at −0.4 V which is characteristic of neutral TPB. The increase in the oxidation potential above 0.26 V is associated with the development of two new bands appearing at 476 nm and 1083 nm, which can be assigned to the HOMO–SOMO and SOMO–LUMO transitions of the radical cation (Fig. S13b, ESI†).[42,48] The intensity of these bands reaches a maximum at 0.6 V (purple line) after which a band with an absorption maximum at 741 nm starts forming, while the neutral band reaches its minimum. The band at 741 nm is – in accordance with the literature – assigned to the dication TPB^{2+} species. Two sets of isosbestic points are encountered: at 395 nm for $TPB/TPB^{+\bullet}$, and at 378 nm, 425 nm, 529 nm and 995 nm for the redox couple $TPB^{+\bullet}/TPB^{2+}$. The onset for the peak-trend in the forward oxidation cycle (Fig. S13d, ESI†) coincides also with the conductance onset (Fig. 2b). The conductance profile in the forward cycle shows a bell-shape with a maximum at 0.57 V and a shoulder around 0.42 V, no conductance is measured up to 0.2 V and above 0.8 V. This behavior can be explained by mixed-valence conductivity.[9] The polymer conductance only starts increasing above 0.2 V due to the hopping between neutral and radical cation species. The first shoulder is reached at 0.42 V in close correspondence to the half-wave potential for the first oxidation ($E^{1/2}$ ($TPB/TPB^{+\bullet}$)) in the CV. The conductance then further increases reaching its highest value at 0.57 V which is around the half-wave potential for the second oxidation ($E^{1/2}$ ($TPB^{+\bullet}/TPB^{2+}$)). Upon further increasing the potential the conductance decreases, as at some point only TPB^{2+} species are available, *i.e.* no more sites for electron hopping. This conductance behavior was already described by Yurchenko *et al.*[34] in terms of two distinct but partially overlapped conductance regimes where hopping takes place between the two redox couples of TPB.[7,8] Interestingly, in the literature example the authors found two independent conductance maxima of equal intensity. Our data however show a broader and barely resolved conductance regime with a higher conductance registered for the $TPB^{+\bullet}/TPB^{2+}$ redox couple. We suggest that these differences might arise from the slightly different chemical nature of the two polymers under study. Whereas in our case the TPA redox units are directly connected to a polyvinyl backbone, in the case of Yurchenko *et al.* the pendant TPA units were linked *via* oxydimethylene spacers to a polystyrene backbone. We suggest that the different extent of interactions between the redox units in the two polymer films might result in the variations of the local environments of the redox centers, giving rise to slightly different ranges of redox potentials[8,49–52] and, consequently, to the observed differences in the conductance profiles.

Poly(BPhCbz)

Fig. 3a and b show the spectra and conductance which were registered during the charging of poly(BPhCbz) in the forward cycle. The complete datasets can be found in the ESI† (Fig. S14 and S15). The neutral state of poly(BPhCbz) is characterized by a λ_{max} of 326 nm. The radical cation state has two characteristic bands at 426 nm and 1047 nm and the dication state gives a

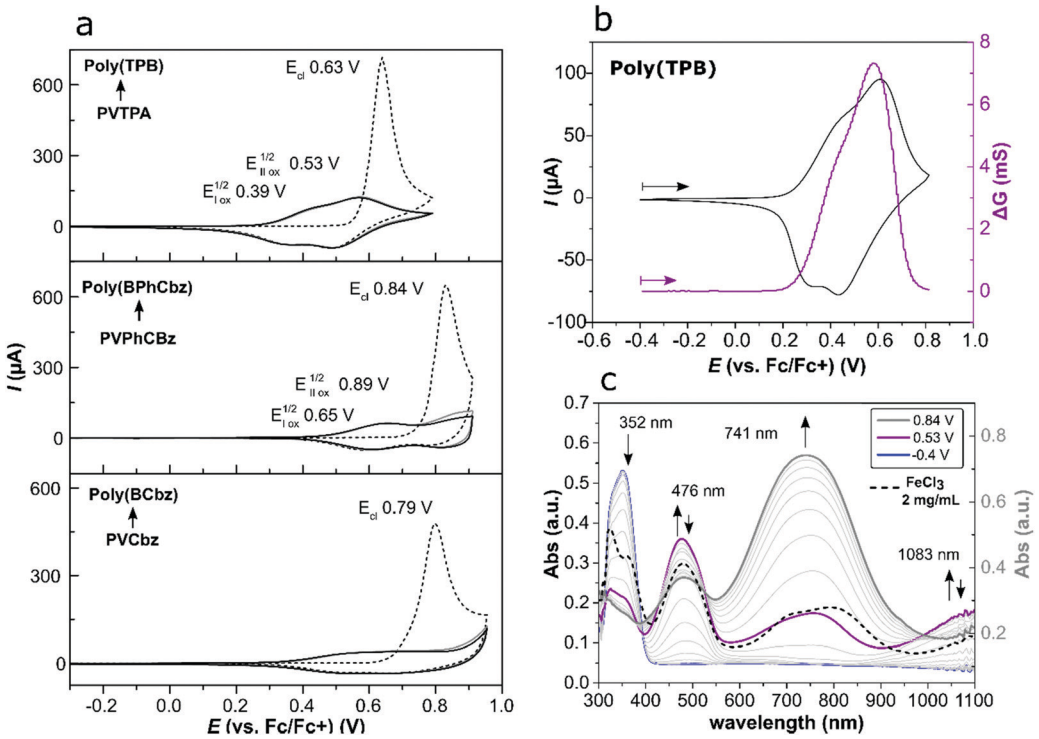

Fig. 2 (a) CV pattern for three subsequent oxidative cycles of PVTPA, PVPhCbz and PVCbz thin polymer films registered in 0.1 M Bu_4NPF_6/CH_3CN with a scan rate of 20 mV s^{-1}. The first cycle is indicated with a dashed line, the second cycle with a gray line and the third cycle with a continuous black line. After the first cycle poly(TPB), poly(BPhCbz) and poly(BCbz) are generated. (b) and (c) CV coupled with *in situ* conductance (b) and *in situ* spectroscopy (c) of poly(TPB) in 0.1 M Bu_4NPF_6/CH_3CN with a scan rate of 20 mV s^{-1}. The conductance change during the forward cycle is indicated by a continuous purple line in (b). The purple line in (c) shows an absorption spectrum taken at 0.53 V. For comparison reasons the black dashed line (right *y*-axis) in (c) shows the absorption spectrum of a PVTPA film which was chemically doped by 2 mg mL^{-1} $FeCl_3$ which gives the maximum conductivity registered during the chemical doping experiment (compare Fig. 1).

λ_{max} of 758 nm. Isosbestic points for the redox couple BPhCbz/$BPhCbz^{+\bullet}$ are found at 355 nm and for $BPhCbz^{+\bullet}/BPhCbz^{2+}$ at 466 nm and 995 nm.[53] The UV-Vis-NIR spectroscopic assignments are also supported by EPR data in the literature.[22,54] In Fig. 3a the absorption spectra registered for the potential values associated with the two conductance maxima (0.67 V, green) and (0.89 V, purple) in Fig. 3b are highlighted. The peak evolution for the different doped states in Fig. 3b shows the increase in absorption of the radical cation state (green curves, 426 and 1047 nm) together with the absorption decrease of the neutral band starting from 0.42 V which coincides with the onset of the *in situ* conductance and the oxidation onset (see the CV trace in Fig. S14, ESI†). The maximum absorption (*i.e.* concentration) of the radical cation is reached at 0.80 V, the potential value at which the dication band intensity also starts to increase. This potential value correlates well with the relative minimum between the two conductance maxima in the *in situ* conductance plot (black curve, Fig. 3a).

The behaviour of poly(BPhCbz) is overall very similar to the poly(TPB) film with bell-shaped conductance and presence of two defined mixed conducting regimes and higher conductance when $BPhCbz^{+\bullet}/BPhCbz^{2+}$ species are present. Another interesting observation concerns the lower conductance associated to electron hopping between $N/R^{+\bullet}$ and $R^{+\bullet}/D^{2+}$ found for poly(TPB) and poly(BPhCbz). In both cases the conductance for the second conductance regime is around twice as high as the first one. Similar findings are also described for oligothiophenes in the literature.[13,55] The results could be explained by a different electron diffusion coefficient for the different species ($N/R^{+\bullet}$) < ($R^{+\bullet}/D^{2+}$). Another possible explanation could be the superimposition of the second regime upon the first due to the small peak to peak separation of only 140 mV in the case of poly(TPB) and 210 mV in poly(BPhCbz).

Poly(BCbz)

In situ UV-Vis-NIR spectra registered during the forward CV cycle of poly(BCbz) are presented in Fig. 3c (and Fig. S16 & S17, ESI†). In accordance with the other two polymers we assign the following redox states: 326 nm for the neutral polymer; broad bands around 400 nm and above 1000 nm for the radical cation and another broad band with a maximum at 761 nm for the dication. In this case only a single isosbestic point at 966 nm is visible. With respect to the two other polymers, the spectroscopic variation between the different redox states seems to be less pronounced. This also becomes evident from the peak-evolution in Fig. 3d. In the case of poly(BCbz) the radical cation bands (green curves, 402 nm and 999 nm) do not decrease in intensity after the first oxidation is completed, but seem to rather reach saturation for higher potentials. These absorption variations also correlate well with the *in situ* conductance

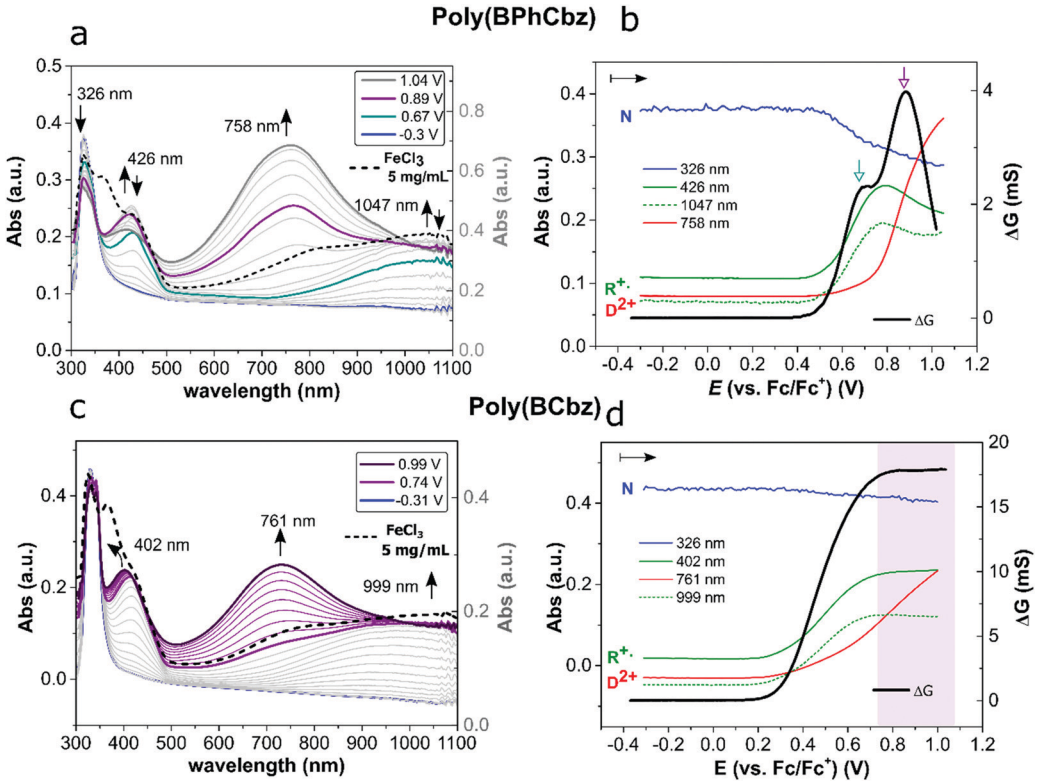

Fig. 3 Summary of electrochemical *in situ* conductance and spectroscopy data for poly(BPhCbz) (a and b) and poly(BCbz) (c and d) which were generated according to the protocol in Fig. 2. The measurements were performed in 0.1 M Bu_4NPF_6/CH_3CN with a scan rate of 20 mV s^{-1}. The data are shown for the forward cycle. For full cycles compare the ESI.† (a) and (c) The development of the absorption spectra as a function of potential. Additionally the absorption of the chemically doped films (5 mg mL^{-1} $FeCl_3$) is shown for comparison (right *y*-axis). (b) and (d) The conductance profiles and the peak trends of selected wavelengths for the neutral species (blue), radical cation (green) and dication (red) species from (a) and (c).

measurement, Fig. 3d. By increasing the polymer oxidation level, the conductance slowly starts to increase above 0.18 V as radical cations are generated (development of the 402 and 999 nm bands, green curves). Above 0.7 V the radical cation absorption saturates and in correspondence to the slope change in the dication band at 761 nm (red curve), the film reaches its maximum conductance. This maximum conductance is maintained throughout the entire potential window explored (up to 1.1 V).

Despite their structural similarities it is striking that poly(BCbz) shows a significantly different conductance profile compared to poly(TPB) and poly(BPhCbz). Whereas two conductance regimes with the corresponding maxima could be identified for poly(TPB) and poly(BPhCbz), the conductance trend in the case of poly(BCbz) shows a broad region of high conductance. Such a conductance plateau is usually reported for conjugated polymers, and has not been reported for redox systems so far.[7,8] Furthermore, in analogy to conjugated systems the voltammogram of poly(BCbz) appears featureless (Fig. 4b, see discussion below).

Discussion

PVTPA and PVPhCbz films with bell-shape conductivity

From the comparison of the electrochemical results with the spectroscopic and conductivity study of chemically doped PVTPA and PVPhCbz films, we find that the doping with the $FeCl_3$ dopant leads to highly conducting states only when charge carriers of different oxidation states are concurrently present. This is the case for the PVTPA and PVPhCbz films for doping with 2 and 5 mg mL^{-1} respectively, where the highest conductivities of the two polymer films are registered (Fig. 1). For a direct comparison, we superimposed the absorption of the chemically oxidized samples at their maximum conductivity with the ones registered during the spectroelectrochemical measurements, compare Fig. 2c for poly(TPB) and Fig. 3b for poly(BPhCbz). In both cases the samples are characterized by the simultaneous presence of radical cation and dication species. By comparing the film absorption maxima of the different states of oxidation obtained by chemical and electrochemical doping, the absorption peak maxima for the different states of oxidation are well comparable between chemically and electrochemically oxidized samples. The maxima after $FeCl_3$ doping show only a slight blue shift with respect to the electrochemically doped samples (Table 1). Similar observations were also found for polaron and bipolaron band positions in various conjugated polymers and are generally discussed in terms of polaron/bipolaron-anion distance resulting from different counterions. In our case the differences observed might arise from the slightly larger thermochemical radius *r* of $FeCl_4^-$ (r = 3.35 Å) compared to PF_6^- (r = 2.4 Å) as counteranions.[56–58]

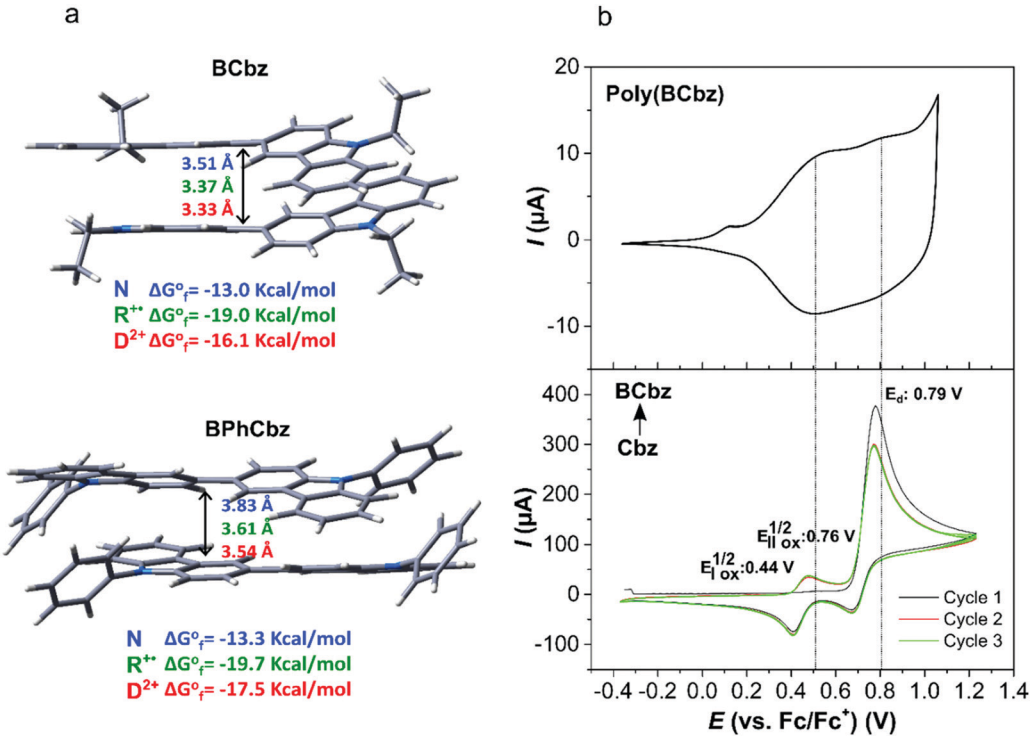

Fig. 4 (a) Lateral views of the DFT-computed global minimum structure π-dimers of BCbz and BPhCbz in an anti configuration. The shortest C–C distances between the monomers and the free energy of formation values (at 298 K) calculated at the ωB97XD/6-31G** level in acetonitrile are also shown (blue, green and red values denoted the neutral, radical cation and dication states, respectively). (b) CV of poly(BCbz) in 0.1 M Bu_4NPF_6/CH_3CN, scan rate 20 mV s^{-1}, film prepared according to the protocol in Fig. 2a. (c) CV of *N*-ethyl carbazole (0.5 mM) in 0.1 M Bu_4NPF_6/CH_3CN, scan rate 150 mV s^{-1}; Au working electrode.

In the case of chemical doping there might always be the issue of no complete crosslinking of films. An additional voltammetric characterization of chemically doped PVTPA samples hints in this direction (Fig. S4, ESI†). Overall higher oxidant concentrations would be necessary to trigger the crosslinking and doping of PPhCbz film, which seems to be in accordance with the higher oxidation potential of PVPhCbz (0.84 V) with respect to PVTPA (0.63 V). The oxidation potential of $FeCl_3$ is *ca.* 1.47 V *vs.* $Fc|Fc^+$,[35] which indicates the thermodynamic feasibility of the oxidation of the polymer films. Furthermore, diffusion of the oxidant through the polymer film must, however, be taken into consideration as well.

One aspect regarding air stability shall be mentioned here as well: we found that highly oxidized, but low conducting PVTPA films (*e.g.* after $FeCl_3$ doping with 4 mg mL^{-1} for 10 s with conductivities of 10^{-5} S cm^{-1}) undergo a dedoping process upon contact with air, probably due to interaction with air moisture, Fig. S1 (ESI†). These films then show high conductivity values in the range of 10^{-3} S cm^{-1}, which means that after dedoping conductivities are reached in air which are comparable to the peak conductivities for PVTPA measured in the glovebox (when exposed to 2 mg mL^{-1} $FeCl_3/CH_3CN$ for 10 s, Fig. 1). UV-Vis-NIR measurements after dedoping indicate coexistence of radical cation and dication species which is optimal for high conductivities. The stability of the doped states upon prolonged contact with air will be further explored.

Chemical doping of PVTPA and PVPhCbz and in particular the conductivity profiles can overall be well compared with the *in situ* experiments and the conductivity behavior can be explained by mixed valence conductivity.[7,9] As already discussed, the model predicts that for localized electroactive system conductivity is sustained by the electron hopping between redox units in different states of oxidation. The highest conductivity for a certain redox event is found at its half-wave potential. In this situation the highest probability for electron hopping is found when exactly half of the redox states for the redox reactions are occupied.[7,8,10,59] A model of mixed conductivity is given in Scheme 1b.

PVCbz: plateau conductivity

In contrast to the bell-shape discussed above, both chemical and electrochemical doping experiments of the PVCbz films indicate a conductivity/conductance plateau maintained over the whole concentration and potential range analyzed. This is surprising due to the structural similarities between the 3 polymers, all characterized by pendant dimeric redox units that can be reversibly oxidized in two redox steps. Such plateau conductivity has so far only been observed in conjugated polymer films, such as poly(3-hexylthiophene) (P3HT) and PEDOT.[7,12,18,28] Electron hopping between polymer chains generally constitutes the rate determining step for charge transport in conducting polymers. In this context, high conducting

states can for example be achieved by favoring the spatial proximity of the redox units for an efficient electron tunneling and by a low reorganization energy.[8,9,14,60] π-dimers and π-stacks are known to favor interchain transport of charge carriers in conjugated polymers.[8,49,61–63] It was also recently found that an effective π–π stacking constitutes the bottle-neck to enhance the electrical performance of conducting polymers allowing for good percolation channels, rather than high crystallinity and high order.[64,65] Zozoulenko *et al.* analyzed the charge percolation efficiency in different PEDOT:tosylate morphologies, showing how samples with relatively low order but with good π–π connections between the polymer chains are more efficient connections for charge hopping than disjunct crystallites in highly crystalline samples. Similar considerations resulted in a very recent work from our group; we measured surprisingly high conductivities in simply spin-coated disordered P3HT films using an *ex situ* electrochemical doping approach.[22]

To get more insight into the difference between the systems, we carried out DFT calculations to investigate the ability for π-dimer formation and π–π aggregates comparing pure BPhCbz and BCbz dimer systems. Since TPB is a propeller-like structure with limited ring planarization and low tendency to π-stacking,[27] this system was not taken further into consideration. Two different cofacial arrangements of the BPhCbz and BCbz moieties were considered: a parallel (*syn*) and an antiparallel (*anti*) conformation. The negative Gibbs free energy values reveal the favourable formation of π–π aggregates in the neutral, radical cation and dication states, both in the BPhCbz and BCbz systems (Fig. 4 and Fig. S22, ESI†). The *anti* configuration is found to be 2–3 kcal mol^{-1} more stable than the parallel *syn* model, with similar energies found for BPhCbz and BCbz systems. Smaller intermolecular π-stacking distance and a higher cofacial overlap are calculated for BCbz compared to BPhCbz (Fig. 4 and Fig. S22–S25, ESI†).

A stronger interaction between the BCbz units is further corroborated by the experimental spectroscopic data: the absence of an isosbestic point and the merging of the radical cation and dication bands might suggest overall less defined distinction between the redox states. Also the electrochemical characterization of poly(BCbz) does point in this direction. The CV in Fig. 4b is rather featureless and capacitive with several broad overlapping redox waves. It is quite usual to find that the shapes of CVs are strongly dependent on intermolecular interactions.[66] Reciprocal interactions, differences in the spatial distribution of the redox centers and a distribution of species with different E^0 can give rise to peak widths at half-height that can differ by up to several hundreds of mV from the theoretically expected value of 90.6 mV for the one electron exchange of surface confined species at RT.[8,49–52] For comparison reasons we did a CV analysis of the low molecular compound *N*-ethylcarbazole presented in Fig. 4c. The two broad redox waves that can be identified over the broad CV signal of poly(BCBz) correlate in potential values with the first and second oxidation of the dimer of *N*-ethylcarbazole registered during the CV experiments (Fig. 4 and Fig. S9, ESI†). The electrolysis of *N*-ethylcarbazole performed in solution with similar conditions to the electrochemical polymer film oxidation (the same electrolyte and electrode support, Fig. S8 and S9, ESI†) confirms literature results which claim the formation of only dimeric species and no higher oligomers with the experimental conditions employed.[37,40] In this context, the featureless CV and wider electrochemical window of poly(BCbz) with respect to the other polymers analysed in the manuscript could be described as a result of the conspicuous intermolecular interactions which might arise from a more efficient π-stacking. One could consider the redox polymers, despite the limited conjugation length of the dimers, as a network of close interacting dimers which generate a band of closely spaced states with slightly different energies. These could be considered as several close redox states and conductivity described as discussed earlier by Heinze *et al.*[7] as a sequence of electron hopping between several mixed valence-states very close in energy. Analogous considerations were proposed by Zotti *et al.*[67] to describe the plateau conductivity found for octathiophene and decathiophene oligomers despite their limited conjugation.

In the case of conjugated polymers and oligomers the separation between *intra-* and *inter*-molecular contributions to conductivity is usually non-trivial because of their strict interrelation. Since we compare redox systems characterized by a limited and comparable conjugation of the redox units[36,37,47] we can consider that the observed modifications of conductivity trends are mainly determined by the different degrees of inter-chain interactions encountered in the systems. The experimental results show that an efficient cross-communication allowing three-dimensional electronic connectivity for hopping strongly affects the conductivity profile, which results for poly(BCbz) in a broader region of higher plateau-like conductance also for higher doping levels, normally found for conjugated systems. Similar considerations were used by Swager *et al.*[14] to explain the differences in the potential-dependent conductivities of a polypyrrole substituted with bulky canopy units with respect to unsubstituted polypyrrole. The authors observed how the reduced cross-communication between adjacent polymer strands results in a bell-shaped profile in the *in situ* conductance with respect to the normal plateau like behavior observed in the unsubstituted polypyrrole.

Maximum conductivities

Remarkably, the conductivity of PVCbz after $FeCl_3$ doping results in maximum conductivities as high as 2×10^{-2} S cm^{-1} which are maintained over different levels of oxidation of the polymer. Also the conductivities obtained with the described doping procedure for PPhCbz and PVTPA with 10^{-3} S cm^{-1} are high for this class of polymers. Compared to the literature the conductivity values are higher than the ones reported for chemically doped PVCbz.[68–71] Kanega *et al.* reached conductivities of up to 6×10^{-4} S cm^{-1}[68] upon oxidation with $SbCl_5$, while Block *et al.*[71] reported 10^{-5} S cm^{-1} by doping to BCz radical cations (stoichiometric determination) with tris(4-bromophenyl)ammoniumyl hexachloroantimonate. One possible reason for these lower values could be that the doping in these studies only resulted in a radical cation state, as demonstrated by optical absorption. Our

data on the other hand suggest that the highest conductivity values should only be reached when also some of the redox active units are oxidized to the dication level. This result emphasizes the importance of performing electrochemical and chemical doping studies in parallel as it helps to target the doping process towards the highest conducting state for the system. Other very recent literature also points in this direction.[22,56]

Just to mention some other conductivities of redox polymers from the literature: polymers bearing the redox-active unit 2,2,6,6-tetramethylpiperidinyloxyl (TEMPO) as a pendant can reach maximum conductivies as high as 8.5×10^{-3} S cm^{-1} upon electrochemical doping.[72,73] Tetrathiafulvalene (TTF) based redox polymers did show conductivities up to 2.3×10^{-3} S cm^{-1} upon doping with tetracyanoquinodimethane.[74,75] Furthermore, TPA based films for optical applications showed upon doping maximum conductivities of the order 10^{-3}–10^{-2} S cm^{-1}.[31,76,77] Finally, also in the case of chemical doping of the n-type polymer PNDI2OD-T2 values of 10^{-3}–10^{-2} S cm^{-1} are found, *i.e.* a similar order of magnitude.[23,24]

In general redox polymers present conductivities which are orders of magnitude lower than those reachable by conjugated systems. However, also the chemical nature might play a role: while PVCbz can give 2.1×10^{-2} S cm^{-1} as reported here, the conjugated carbazole analog poly(3,6-*N*-alkylcarbazole) gives maximum conductivities of 1 S cm^{-1} [43,78,79] which are still orders of magnitude smaller than classical polythiophenes such as P3HT or PEDOT with conductivities ranging from hundreds to thousands of S cm^{-1}. We might guess that preparing redox polymers based on oligothiophene pendant groups which have strong intermolecular interactions might also show higher values. This will be the subject of further studies.

Conclusions

In conclusion, we presented a study on electronic conductivity upon chemical and electrochemical oxidation of polyvinyltriphenylamine (PVTPA) and polyvinylcarbazole (PVPhCbz and PVCbz) redox polymer films. The oxidative dimerization of the electroactive units is performed on solution cast films and results in polymer crosslinking. Upon exposure to $FeCl_3$ solutions highly conducting films are obtained with maximum conductivities ranging from 10^{-3} to 10^{-2} S cm^{-1}. The increased chemical stability resulting from crosslinking together with the transparency of the conducting layers makes them interesting candidates for optoelectronic applications as HTLs or transparent electrodes.

We found that doping of PVTPA and PVPhCbz gives bell-shaped conductivity profiles with a maximum conductivity only observed when radical cations and dications are both present with the pure neutral and fully oxidized samples only giving very low conductivities. Crosslinked and doped PVCbz films on the other hand do maintain the highest conductivity over a broad doping range of 400 mV (from 0.7 to 1.1 V) and a range of doping concentrations. This is also the region where dication species are concurrently present with radical cations.

The bell-shape conductivity profile also implies that for chemical doping the exact doping concentration has to be found, while the plateau-conductivity is overall less sensitive to the doping conditions. *In situ* electrochemistry with conductance and spectroscopy proved to be useful to identify the right doping regime targeted. We suggest that efficient cross-communication allowing three-dimensional electronic connectivity for hopping strongly affects the conductivity profile in the case of doping PVCbz. DFT calculations hint to a pronounced tendency of the bicarbazole units to form π-stacks, and in particular, in the case of BCbz smaller intermolecular π-stacking distances are calculated in comparison to BPhCbz. A more efficient π-stacking between neighboring units may explain the broad region of high conductivity. Summarizing, designing redox polymers with efficient spatial interactions which allow for good hopping connectivities could lead to a broader region of conductivities, similarly to conjugated polymers, with the advantage of a superior redox activity and processability characteristic of these systems.

Conflicts of interest

There are no conflicts to declare.

Acknowledgements

We thank Luca Scapinello and Philipp Sliskovic for the polymer synthesis of PVTPA and PVPhCbz. Discussions and technical support from David Neusser, Sherri Liu and Lukas Stein are highly acknowledged. The work at the University of Stuttgart was funded by IQST (Integrated Quantum Science and Technology) through the Carl Zeiss Foundation. Further funding by the Deutsche Forschungsgemeinschaft (DFG, German Research Foundation) – Project-ID 358283783 – SFB 1333 is highly acknowledged. The work at the University of Málaga was funded by the MINECO (CTQ2015-66897), MICINN (PID2019-110305GB-I00) and by the Junta de Andalucıa (P09-FQM-4708, UMA18-FEDERJA-080). S. G. V. thanks the MINECO for a FPU predoctoral fellowship (FPU 17/04908). The authors thankfully acknowledge the computer resources, technical expertise, and assistance provided by the SCBI (Supercomputing and Bioinformatics) center of the University of Málaga.

References

1 J. Reynolds, B. C. Thompson and T. A. Skotheim, *Handbook of Conducting Polymers*, 4th edn, 2019.
2 S. Mukherjee and B. W. Boudouris, *Organic Radical Polymers: New Avenues in Organic Electronics*, 2017.
3 W. T. Neo, Q. Ye, S. J. Chua and J. Xu, *J. Mater. Chem. C*, 2016, **4**, 7364–7376.
4 M. E. Abdelhamid, A. P. O'Mullane and G. A. Snook, *RSC Adv.*, 2015, **5**, 11611–11626.

5 M. Goel and M. Thelakkat, *Macromolecules*, 2020, **53**, 3632–3642.
6 G. Inzelt, *Monographs in Electrochemistry*, 2008.
7 J. Heinze, B. A. Frontana-Uribe and S. Ludwigs, *Chem. Rev.*, 2010, **110**, 4724–4771.
8 T. M. Swager, *Macromolecules*, 2017, **50**, 4867–4886.
9 C. E. D. Chidsey and R. W. Murray, *J. Phys. Chem.*, 1986, **90**, 1479–1484.
10 E. F. Dalton, N. A. Surridge, J. C. Jernigan, K. O. Wilbourn, J. S. Facci and R. W. Murray, *Chem. Phys.*, 1990, **141**, 143–157.
11 G. Schiavon, S. Sitran and G. Zotti, *Synth. Met.*, 1989, **32**, 209–217.
12 G. Salinas and B. A. Frontana-Uribe, *ChemElectroChem*, 2019, 1–14.
13 H. John, R. Bauer, P. Espindola, P. Sonar, J. Heinze and K. Müllen, *Angew. Chem., Int. Ed.*, 2005, **44**, 2447–2451.
14 D. Lee and T. M. Swager, *J. Am. Chem. Soc.*, 2003, **125**, 6870–6871.
15 T. V. Richter, C. H. Braun, S. Link, M. Scheuble, E. J. W. Crossland, F. Stelzl, U. Würfel and S. Ludwigs, *Macromolecules*, 2012, **45**, 5782–5788.
16 S. Link, T. Richter, O. Yurchenko, J. Heinze and S. Ludwigs, *J. Phys. Chem. B*, 2010, **114**, 10703–10708.
17 G. Zotti, G. Schiavon, A. Berlin and G. Pagani, *Synth. Met.*, 1993, **61**, 81–87.
18 M. Wieland, C. Malacrida, Q. Yu, C. Schlewitz and L. Scapinello, *Flex. Print. Electron.*, 2020, **5**, 014016.
19 A. Smie and J. Heinze, *Angew. Chem., Int. Ed. Engl.*, 1997, **36**, 363–367.
20 D. Ofer, R. M. Crooks and M. S. Wrighton, *J. Am. Chem. Soc.*, 1990, **112**, 7869–7879.
21 J. L. Bredas and G. B. Street, *Acc. Chem. Res.*, 1985, **18**, 309–315.
22 D. Neusser, C. Malacrida, M. Kern, Y. Gross, J. van Slageren and S. Ludwigs, *Chem. Mater.*, 2020, **32**, 6003–6013.
23 Y. M. Gross, D. Trefz, C. DIngler, D. Bauer, V. Vijayakumar, V. Untilova, L. Biniek, M. Brinkmann and S. Ludwigs, *Chem. Mater.*, 2019, **31**, 3542–3555.
24 D. Trefz, A. Ruff, R. Tkachov, M. Wieland, M. Goll, A. Kiriy and S. Ludwigs, *J. Phys. Chem. C*, 2015, **119**, 22760–22771.
25 G. Jiang, C. Huang, A. Baba and R. Advincula, *Macromol. React. Eng.*, 2012, **6**, 153–159.
26 A. Baba, K. Onishi, W. Knoll and R. C. Advincula, *J. Phys. Chem. B*, 2004, **108**, 18949–18955.
27 P. Blanchard, C. Malacrida, C. Cabanetos, J. Roncali and S. Ludwigs, *Polym. Int.*, 2019, **68**, 589–606.
28 P. Reinold, K. Bruchlos and S. Ludwigs, *Polym. Chem.*, 2017, **8**, 7351–7359.
29 E. J. W. Crossland, P. Cunha, S. Scroggins, S. Moratti, O. Yurchenko, U. Steiner, M. A. Hillmyer and S. Ludwigs, *ACS Nano*, 2010, **4**, 962–966.
30 J. Kim, J. H. Kim and K. Ariga, *Joule*, 2017, **1**, 739–768.
31 J. Liu, W. Liu, E. Aydin, G. T. Harrison, F. H. Isikgor, X. Yang, A. S. Subbiah and S. De Wolf, *ACS Appl. Mater. Interfaces*, 2020, **12**, 23874–23884.
32 X. Gu, Y. Li, Y. Mu, M. Zhang, T. Lu and P. Wang, *RSC Adv.*, 2018, **8**, 9409–9413.
33 B. Lüssem, M. Riede and K. Leo, *Phys. Status Solidi A*, 2013, **210**, 9–43.
34 O. Yurchenko, J. Heinze and S. Ludwigs, *ChemPhysChem*, 2010, **11**, 1637–1640.
35 B. Kratochvil and R. Long, *Anal. Chem.*, 1970, **42**, 43–46.
36 M. Li, *Chem. – Eur. J.*, 2019, **25**, 1142–1151.
37 S. Mallick, S. Maddala, K. Kollimalayan and P. Venkatakrishnan, *J. Org. Chem.*, 2019, **84**, 73–93.
38 C. Su, Y. Ye, L. Xu and C. Zhang, *J. Mater. Chem.*, 2012, **22**, 22658–22662.
39 A. Maity and M. Biswas, *J. Appl. Polym. Sci.*, 2006, **100**, 819–824.
40 K. Karon and M. Lapkowski, *J. Solid State Electrochem.*, 2015, **19**, 2601–2610.
41 P. Reiser, L. Müller, V. Sivanesan, R. Lovrincic, S. Barlow, S. R. Marder, A. Pucci, W. Jaegermann, E. Mankel and S. Beck, *J. Phys. Chem. C*, 2018, **122**, 14518–14527.
42 O. Yurchenko, D. Freytag, L. Zur Borg, R. Zentel, J. Heinze and S. Ludwigs, *J. Phys. Chem. B*, 2012, **116**, 30–39.
43 C. Chevrot, E. Ngbilo, K. Kham and S. Sadki, *Synth. Met.*, 1996, **81**, 201–204.
44 V. Carlier, M. Skompska and C. Buess-Herman, *J. Electroanal. Chem.*, 1998, **456**, 139–152.
45 R. F. Nelson and R. N. Adams, *J. Am. Chem. Soc.*, 1968, **90**, 3925–3930.
46 J. F. Ambrose and R. F. Nelson, *J. Electrochem. Soc.*, 1969, **115**, 1159–1164.
47 C. Malacrida, A. Hossein, S. Gámez-Valenzuela, I. Lenk, P. Simon, A. Labrunie, J. Grolleau, J. T. López Navarrete, M. C. Ruiz Delgado, C. Cabanetos, P. Blanchard and S. Ludwigs, *ChemElectroChem*, 2019, 1–15.
48 P. Rapta, J. Lukkari, J. Tarábek, M. Salomäki, M. Jussila, G. Yohannes, M. L. Riekkola, J. Kankare and L. Dunsch, *Phys. Chem. Chem. Phys.*, 2004, **6**, 434–441.
49 R. Takita, C. Song and T. M. Swager, *Org. Lett.*, 2008, **10**, 5003–5005.
50 R. G. Compton, M. E. Laing, A. Ledwith and I. I. Abu-Abdoun, *J. Appl. Electrochem.*, 1988, **18**, 431–440.
51 P. J. Peerce and A. J. Bard, *J. Electroanal. Chem.*, 1980, **114**, 89–115.
52 N. Kurapati, P. Pathirathna, R. Chen and S. Amemiya, *Anal. Chem.*, 2018, **90**, 13632–13639.
53 C. L. Ramírez, M. I. Mangione, S. G. Bertolotti, E. M. Arbeloa and A. R. Parise, *J. Photochem. Photobiol., A*, 2018, **365**, 199–207.
54 M. Lapkowski, J. Zak, K. Karon, B. Marciniec and W. Prukala, *Electrochim. Acta*, 2011, **56**, 4105–4111.
55 T. Benincori, S. Gámez-Valenzuela, M. Goll, K. Bruchlos, C. Malacrida, S. Arnaboldi, P. R. Mussini, M. Panigati, J. T. López Navarrete, M. C. Ruiz Delgado, G. Appoloni and S. Ludwigs, *Electrochim. Acta*, 2018, **284**, 513–525.
56 A. I. Hofmann, R. Kroon, S. Zokaei, E. Järsvall, C. Malacrida, S. Ludwigs, T. Biskup and C. Müller, *Adv. Electron. Mater.*, 2020, 2000249.
57 V. Vijayakumar, Y. Zhong, V. Untilova, M. Bahri, L. Herrmann, L. Biniek, N. Leclerc and M. Brinkmann, *Adv. Energy Mater.*, 2019, **9**, 1–12.

58 Z. Liang, Y. Zhang, M. Souri, X. Luo, A. M. Boehm, R. Li, Y. Zhang, T. Wang, D. Y. Kim, J. Mei, S. R. Marder and K. R. Graham, *J. Mater. Chem. A*, 2018, **6**, 16495–16505.
59 H. John, R. Bauer, P. Espindola, P. Sonar, J. Heinze and K. Müllen, *Angew. Chem., Int. Ed.*, 2005, **44**, 2447–2451.
60 R. Shomura, K. Sugiyasu, T. Yasuda, A. Sato and M. Takeuchi, *Macromolecules*, 2012, **45**, 3759–3771.
61 Y. Harima, X. Jiang, Y. Kunugi, K. Yamashita, A. Naka, K. K. Lee and M. Ishikawa, *J. Mater. Chem.*, 2003, **13**, 1298–1305.
62 K. M. Knoblock, C. J. Silvestri and D. M. Collard, *J. Am. Chem. Soc.*, 2006, **128**, 13680–13681.
63 T. Sakai, T. Satou, T. Kaikawa, K. Takimiya, T. Otsubo and Y. Aso, *J. Am. Chem. Soc.*, 2005, **127**, 8082–8089.
64 N. Rolland, J. F. Franco-Gonzalez, R. Volpi, M. Linares and I. V. Zozoulenko, *Phys. Rev. Mater.*, 2018, **2**, 1–9.
65 S. Wang, S. Fabiano, S. Himmelberger, S. Puzinas, X. Crispin, A. Salleo and M. Berggren, *Proc. Natl. Acad. Sci. U. S. A.*, 2015, **112**, 10599–10604.
66 K. Bruchlos, D. Trefz, A. Hamidi-Sakr, M. Brinkmann, J. Heinze, A. Ruff and S. Ludwigs, *Electrochim. Acta*, 2018, **269**, 299–311.
67 B. G. Zotti, G. Schiavon and A. Berlin, *Adv. Mater.*, 1993, **5**, 551–554.
68 H. Kanega, Y. Shirota and H. Mikawa, *J. Chem. Soc., Chem. Commun.*, 1984, 158–159.
69 J. M. Reyna-González, P. Roquero and E. Rivera, *Des. Monomers Polym.*, 2009, **12**, 233–245.
70 J. V. Grazulevicius, P. Strohriegl, J. Pielichowski and K. Pielichowski, *Prog. Polym. Sci.*, 2003, **28**, 1297–1353.
71 H. Block, M. A. Cowd and S. M. Walker, *Polymer*, 1977, **18**, 781–785.
72 C. Karlsson, T. Suga and H. Nishide, *ACS Appl. Mater. Interfaces*, 2017, **9**, 10692–10698.
73 L. Rostro, S. H. Wong and B. W. Boudouris, *Macromolecules*, 2014, **47**, 3713–3719.
74 Y. Ren and J. S. Moore, *Polym. Chem.*, 2015, **6**, 8325–8330.
75 T. Shimizu and T. Yamamoto, *Chem. Commun.*, 1999, 515–516.
76 N. Mizoshita and S. Inagaki, *Adv. Funct. Mater.*, 2018, **28**, 1803116.
77 Y.-S. Liu, S. Guo, J. Feng, Y.-F. Liu, Y.-G. Bi, D. Yin, X.-L. Zhang and H.-B. Sun, *Opt. Lett.*, 2019, **44**, 4817–4820.
78 S. T. Wellinghoff, Z. Deng, J. F. Reed and S. A. Jenekhe, *Mol. Cryst. Liq. Cryst.*, 1985, **118**, 403–412.
79 S. Wakim, B. R. Aïch, Y. Tao and M. Leclerc, *Polym. Rev.*, 2008, **48**, 432–462.